

# Direct sampling of electric-field vacuum fluctuations

C. Riek, D. V. Seletskiy, A. S. Moskalenko, J. F. Schmidt, P. Krauspe, S. Eckart, S. Eggert, G. Burkard, A. Leitenstorfer\*

The ground state of quantum systems is characterized by zero-point motion. This motion, in the form of vacuum fluctuations, is generally considered to be an elusive phenomenon that manifests itself only indirectly. Here, we report direct detection of the vacuum fluctuations of electromagnetic radiation in free space. The ground-state electric-field variance is inversely proportional to the four-dimensional space-time volume, which we sampled electro-optically with tightly focused laser pulses lasting a few femtoseconds. Subcycle temporal readout and nonlinear coupling far from resonance provide signals from purely virtual photons without amplification. Our findings enable an extreme time-domain approach to quantum physics, with nondestructive access to the quantum state of light. Operating at multiterahertz frequencies, such techniques might also allow time-resolved studies of intrinsic fluctuations of elementary excitations in condensed matter.

Vacuum fluctuations give rise to a variety of phenomena, from spontaneous photon emission (1, 2) and the Lamb shift (3) via the Casimir force (4) to cosmological perturbations (5, 6). Representing the ground state, the quantum vacuum does not possess in density. However, finite noise amplitudes of electric and magnetic fields should exist because of Heisenberg's uncertainty principle. These fluctuations are best explained by analogy with a harmonic oscillator of mass  $m$ , resonance angular frequency  $\Omega$ , and total energy

$$H_{\text{HO}} = \frac{1}{2} \left( \frac{p^2}{m} + m\Omega^2 x^2 \right) \quad (1)$$

Quantization results in noncommuting operators for momentum  $p$  and displacement  $x$ . The Gaussian wave function of the ground state exhibits a root mean square (RMS) standard deviation of  $\Delta x = (\hbar/2\Omega m)^{1/2}$  (7, 8), where  $\hbar$  is the reduced Planck constant. The total energy of a radiation field of wavevector  $\mathbf{k}$  in free space, with electric

and magnetic amplitudes  $E$  and  $B$  (respectively), and vector potential  $\mathbf{A}$  in the Coulomb gauge is (9)

$$H_{\text{RF}} = \frac{\epsilon_0 V}{2} (E^2 + c^2 B^2) + \frac{\epsilon_0 V}{2} (A^2 + c^2 |\mathbf{k} \times \mathbf{A}|^2) \quad (2)$$

Considering one polarization direction and the transverse character of electromagnetic waves, Eq. 1 maps onto Eq. 2 by replacing  $x$  with  $A$  (amplitude of vector potential  $\mathbf{A}$ ),  $m$  with  $\epsilon_0 V (\epsilon_0$ , vacuum permittivity;  $V$ , spatial volume), and  $\Omega$  with  $ck \equiv \Omega$  ( $c$ , speed of light;  $k = |\mathbf{k}|$ ). Instead of  $x$  and  $p$ , an uncertainty product now links  $E$  and  $B$  or the amplitudes and phases of  $E$ ,  $B$ , or  $A$ . An RMS amplitude of vacuum fluctuations  $\Delta A = (\hbar/2\Omega\epsilon_0 V)^{1/2}$  results. In contrast to the mechanical case where  $\Delta x$  is known, understanding  $\Delta A$  is less straightforward: Outside any cavities, there are no obvious boundaries that define a normalization volume  $V$ . This situation raises the question of whether direct measurement of the vacuum field amplitude in free space is physically meaningful and feasible.

The quantum properties of light (10) are typically analyzed either by photon correlation (11, 14), homodyning (15–18), or hybrid measurements (19). In those approaches, information is averaged over multiple cycles, and accessing the vacuum state requires amplification. Femtosecond studies

still rely on pulse envelopes that vary slowly relative to the carrier frequency (20–23). In our work, we directly probed the vacuum noise of the electric field on a subcycle time scale using laser pulses lasting a few femtoseconds. In ultrabroad band electro-optic sampling (24–27), a horizontally polarized electric field waveform (red in Fig. 1A) propagates through an electro-optic crystal (EOX), inducing a change  $\Delta n$  of the linear refractive index  $n_0$  that is proportional to its local amplitude  $E_{\text{THz}}$  (Fig. 1A and fig. S1). The geometry is adjusted so that a new index ellipsoid emerges under  $45^\circ$  to the polarization of  $E_{\text{THz}}$ , with  $n_y$  and  $n_x = n_0 \pm \Delta n$ . An ultrashort optical probe pulse at a much higher carrier frequency  $\nu_p$  (green in Fig. 1A; intensity,  $I_p$ ; electric field,  $E_p$ ) copropagates with  $E_{\text{THz}}$  at a variable delay time  $t_d$ . The envelope of  $I_p$  has to be on the order of half a cycle of light at the highest frequencies  $\Omega/2\pi$  of  $E_{\text{THz}}$  that are detected. We used probe pulses as short as  $t_p = 5.8$  fs, corresponding to less than 1.5 optical cycles at  $\nu_p = 255$  THz (fig. S2). Upon passage through the EOX, the  $x'$  and  $y'$  components of  $E_p$  acquire a relative phase delay proportional to  $\Delta n$  and  $E_{\text{THz}}(t_d)$ . The final polarization state of the probe is analyzed with ellipsometry. The differential photocurrent  $\Delta I/I$  is proportional to the electric field  $E_{\text{THz}}(t_d)$ . We used a radio frequency lock in amplifier (RFLA) for readout.

We adjusted for optimal conditions to measure the vacuum signal by studying classical multiterahertz transients, which were synchronized to the probe (8). In Fig. 1B,  $\Delta I/I$  is plotted in red against delay time  $t_d$ . Figure 1C shows the amplitude spectrum (red) and phase deviations (blue) within  $\pm\pi$ , corroborating calculations (8) of an effective sampling bandwidth of  $\Delta\nu = \Delta\Omega/2\pi = 66$  THz (figs. S3 and S4) around a center frequency of  $\nu_c = \Omega_c/2\pi = 67.5$  THz (free space wavelength  $\lambda_c = 4.4 \mu\text{m}$ ). The electric field amplitude  $\bar{E}_{\text{THz}}(t_d)$  is calibrated using (28–30)

$$\frac{\Delta I}{I} \approx \sin \left( \frac{2\pi \nu_p r_{41} n_0^3 l |R(\Omega_c)|}{c} \bar{E}_{\text{THz}} \right) \approx \frac{2\pi \nu_p r_{41} n_0^3 l |R(\Omega_c)|}{c} \bar{E}_{\text{THz}} \quad (3)$$

$r_{41}$  denotes the electro-optic coefficient, and  $l$  is the thickness of the EOX. The amplitude response  $|R(\Omega_c)|$  includes the pulse duration of the probe and velocity matching to the multiterahertz phase (8). The classical field transient in Fig. 1B was

Department of Physics and Center for Applied Photonics, University of Konstanz, D 78457 Konstanz, Germany.

\*Corresponding author. E-mail: [alfred.leitenstorfer@uni-konstanz.de](mailto:alfred.leitenstorfer@uni-konstanz.de)

sampled with a signal to noise ratio better than  $10^3$  at a RFLA detection bandwidth set to 94 Hz. From the confocal amplitude trace and cross section, we estimated a mean photon number below 900 per pulse. This result proves the capability of our approach to characterize ultrabroadband coherent wave packets containing less than  $10^{-3}$  photons, on average, within 1 s.

But can we directly access the ground state  $\Phi_0$  of the radiation field? With the pump branch switched off, electro optic phase shifts might still be caused by vacuum fluctuations copropagating with the probe. This effect should lead to a statistical distribution of the signal around the average of  $\langle \bar{E}_{\text{vac}} \rangle = 0$ . The ground state expectation value of the squared operator for the

electric field in free space (31) yields the RMS amplitude

$$\begin{aligned} \Delta \bar{E}_{\text{vac}} &= \sqrt{\left\langle \Phi_0 \left| \sum_{\Omega} \sum_{\Omega_c} \frac{\hbar \Omega}{2\epsilon_0 V} (\hat{a}_{\Omega} \hat{a}_{\Omega_c}^\dagger)^2 \right| \Phi_0 \right\rangle} \\ &= \sqrt{\left\langle \Phi_0 \left| \sum_{\Omega=\Omega_c}^{\Omega_c+\Delta\Omega/2} \frac{\hbar \Omega}{2\epsilon_0 V} (-\hat{a}_{\Omega}^2 + \hat{a}_{\Omega} \hat{a}_{\Omega_c}^\dagger + \hat{a}_{\Omega_c}^\dagger \hat{a}_{\Omega} + \hat{a}_{\Omega_c}^{\dagger 2}) \right| \Phi_0 \right\rangle} \\ &= \sqrt{\sum_{\nu}^{\nu_c+\Delta\nu/2} \sum_{\nu_c-\Delta\nu/2}^{\nu} \frac{\hbar \nu}{2\epsilon_0 V}} \quad (4) \end{aligned}$$

$\hat{a}_{\Omega}$  and  $\hat{a}_{\Omega}^\dagger$  are the operators for annihilation and creation of a photon with angular frequency  $\Omega$ , respectively ( $\nu$ , frequency;  $\hbar$ , Planck constant).

Because of the commutation relation  $[\hat{a}_{\Omega}, \hat{a}_{\Omega}^\dagger] = 1$ , only  $\hat{a}_{\nu} \hat{a}_{\nu}^\dagger$  provides a nonvanishing contribution. Summing frequencies over our finite sensitivity interval ensures convergence of Eq. 4. The lateral extension of the volume  $V$  is now identified with the effective cross section  $A_{\text{eff}}$  defined by the Gaussian intensity profile of the near infrared probe beam inside the EOX. Theoretical modeling based on Laguerre Gaussian modes (30) yields  $A_{\text{eff}} = w_0^2 \pi$ , where  $w_0$  is the probe spot radius (8). Because  $V = A_{\text{eff}} L$ , only the length  $L$  remains to be determined. Periodic boundary conditions are applicable when the EOX is short relative to the Rayleigh range of the multiterahertz transverse mode, resulting in a density of free space modes  $L/c$ . Summing over all longitudinal modes within a bandwidth of  $\Delta\nu$  eliminates  $L$ , and we obtain

$$\Delta \bar{E}_{\text{vac}} = \sqrt{\frac{\hbar \nu_c \Delta\nu}{2\pi c n_0 \epsilon_0 w_0^2}} \approx 20.2 \frac{\text{V}}{\text{cm}} \quad (5)$$

A factor of  $n_0^{-1/2}$  accounts for dielectric screening inside the EOX (8). Thus, the vacuum amplitude is maximized when averaging over a minimal space time volume, determined in the transverse directions by  $w_0 = 4.25 \mu\text{m}$  (fig. S5). The longitudinal cross section  $c n_0 / (\nu_c \Delta\nu)$  is defined by the Fourier transform of  $R(\Omega)$ , containing the intensity envelope of the 5.8 fs probe pulse and phase matching conditions within the EOX (8).

Are such fluctuations discernible on top of the shot noise due to the Poissonian photon statistics of the coherent probe? An average number of  $N_p = 5 \times 10^8$  photons detected per pulse causes a relative RMS shot noise current of  $\Delta I_{\text{SN}}/I = N_p^{-1/2}$ . With Eq. 3, we obtain the noise equivalent field

$$\begin{aligned} \Delta E_{\text{SN}} &= \frac{c}{2\pi \nu_p r_{41} n_0^2 L \sqrt{N_p} |R(\Omega_c)|} \\ &= 65.0 \frac{\text{V}}{\text{cm}} \quad (6) \end{aligned}$$

Because the shot noise of the near infrared probe, which is centered around  $\nu_p$ , and the vacuum fluctuations at multiterahertz frequencies  $\Omega$  are uncorrelated with each other and lack spectral overlap, the two contributions add up in quadrature. Therefore, the RMS width of the total detected noise distribution is expected to rise by a factor of

$$\frac{\Delta E_{\text{total}}}{\Delta E_{\text{SN}}} = \frac{\sqrt{\Delta E_{\text{SN}}^2 + \Delta \bar{E}_{\text{vac}}^2}}{\Delta E_{\text{SN}}} = 1.047 \quad (7)$$

corresponding to a 4.7% increase, due to the multiterahertz vacuum noise.

To experimentally access the statistics of the quantum vacuum, we extended the RFLA bandwidth to 1.6 MHz and sampled the probability distribution of the electric field  $P(E_{\text{total}})$  every 5  $\mu\text{s}$ . The contribution of the multiterahertz vacuum can be modified to discriminate against the shot noise baseline by longitudinal or transverse expansion of the probed space time volume (Eq. 5). In the first approach, we decreased  $\nu_c$  and  $\Delta\nu$  by chirping the probe pulse to 100 fs (fig. S3), via

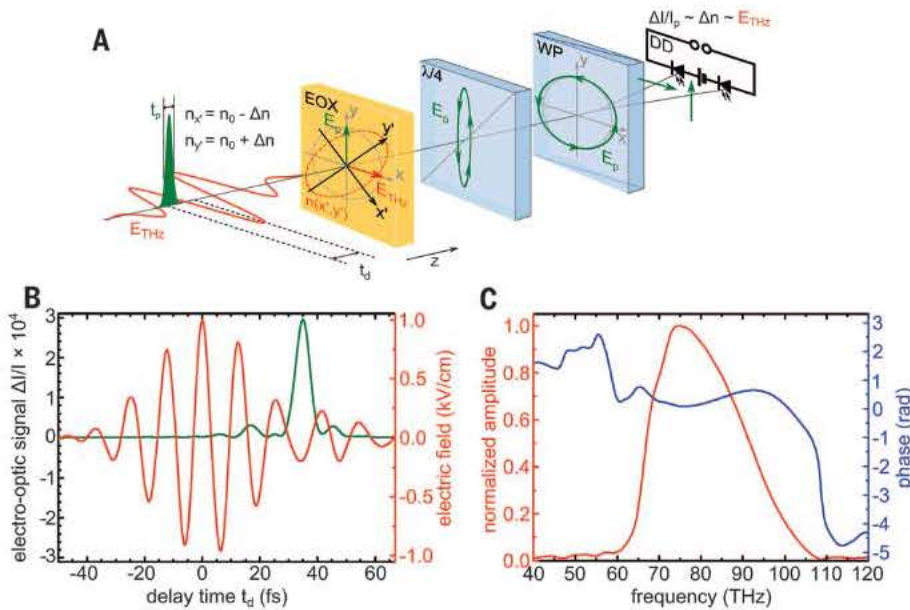


**Fig. 1. Our experimental principle, with a demonstration of ultrahigh bandwidth and sensitivity.**

(A) Scheme of electro-optic sampling of an electric-field waveform (red) by an ultrafast probe pulse (green), consisting of an EOX, a quarter-wave plate ( $\lambda/4$ ), a Wollaston polarizer (WP), and a differential photocurrent detector (DD). (B) Classical electro-optic signal  $\Delta I/I$  and corresponding electric-field amplitude versus delay time  $t_d$  (red line). The intensity envelope of the 5.8-fs probe pulse is shown in arbitrary units for comparison (green line). (C) Spectral multiterahertz amplitude (red) and phase (blue) obtained by Fourier transform.

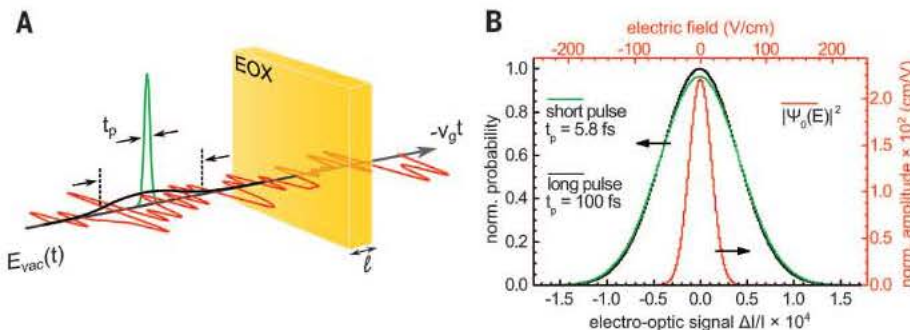


**Fig. 2. Studying vacuum fluctuations via statistic readout and longitudinal modification of the probed space-time volume.**

(A) Diagram showing longitudinal expansion of the probe volume: Stretching the sampling pulse from 5.8 fs (green) to 100 fs (black) causes temporal averaging over the vacuum field (red), leading to a reduction of the detected noise amplitude ( $t_p$ , pulse duration;  $v_g$ , group velocity). (B) Normalized counting probability as a function of electro-optic readout by the short pulse (green) and long pulse (stretched to 100 fs; black). The deconvolved wave function  $|\Psi_0|^2$  of the electric-field ground state is shown in red.

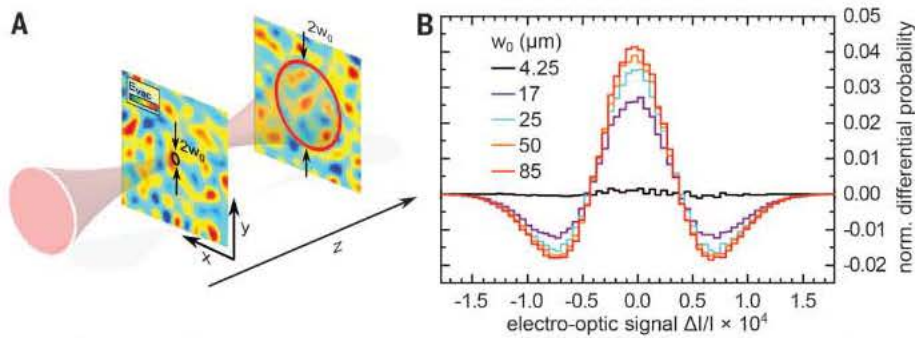


**Fig. 3. Detection by transverse expansion of the space-time segment.** (A) Sketch showing the lateral increase of the sampling cross section, which leads to averaging over noise patterns within the circled areas. (B) Differential histograms obtained by subtracting the result for the confocal detector position with  $w_0 = 4.25 \mu\text{m}$  from the results for positions with the beam diameter at  $4.25 \mu\text{m}$  (black),  $17 \mu\text{m}$  (purple),  $25 \mu\text{m}$  (cyan),  $50 \mu\text{m}$  (orange), and  $85 \mu\text{m}$  (red).

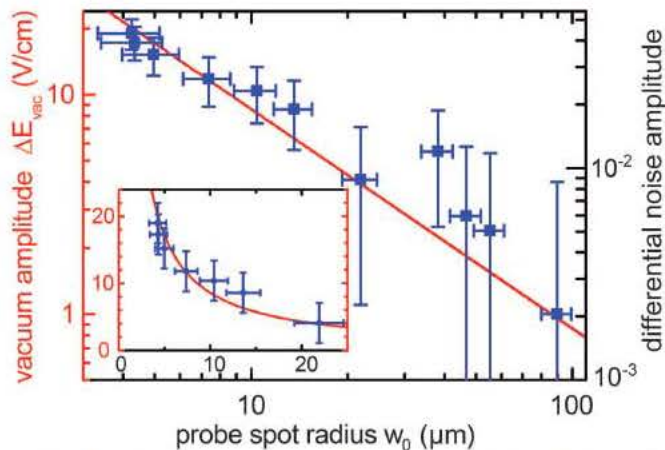


**Fig. 4. Dependence of the vacuum amplitude on transverse extension of the probed space-time volume.** Relative excess noise of electro-optic signal  $\Delta I/I$  (right vertical axis) and RMS vacuum amplitude  $\Delta E_{\text{vac}}$  (left vertical axis) versus probe radius  $w_0$  (blue squares). Red lines represent a theoretical assessment based on Eq. 5.

translation of an SF10 prism in the compressor stage (Fig. 2A). A distinct reduction in peak counts around  $P(E_{\text{total}} = 0)$  is observed when comparing the probability distribution obtained with the 5.8 fs probe (green in Fig. 2B) to the measurement with a stretched pulse (black). Also, the probabilities in the wings of the distribution including the multiterahertz vacuum (5.8 fs probe) are consistently higher than the corresponding values in the stretched pulse distribution. The total change of the normalized noise amplitude amounts to 4%, in good agreement with the theoretical considerations underlying Eqs. 5 to 7. The red histogram in Fig. 2B emerges from a deconvolution algorithm that searches for the best link between distributions of  $P(E_{\text{total}})$  obtained with and without vacuum noise. This result directly mirrors the ground state wave function  $|\Psi_0(E)\rangle^2$  of the electro magnetic field in the polarization plane and space time volume that we probed. From  $|\Psi_0(E)\rangle^2$ , a RMS standard deviation of  $\Delta E_{\text{vac}} = 18 \text{ V/cm}$  is obtained, in good agreement with the theoretical prediction of  $20.2 \text{ V/cm}$  in Eq. 5.

In the transverse option, we kept the short pulse duration and expanded the probe radius  $w_0$  by

translating the EOX out of the confocal plane (Fig. 3A). Averaging over a larger cross section causes a decrease in fluctuation amplitude, which is projected onto the transverse mode of the gate. The effect of progressive narrowing is emphasized with differential probabilities obtained by subtracting a distribution at  $w_0 = 4.25 \mu\text{m}$  from  $P(E_{\text{total}})$  sampled at increasing spot radii (Fig. 3B). When all original histograms are normalized, the maximum change in probability  $\Delta P(E_{\text{total}} = 0)$  of  $0.04 \equiv 4\%$  directly corresponds to the difference between the relative noise amplitudes measured with and without multiterahertz vacuum fluctuations, in quantitative agreement with Eq. 7. The dependence of the vacuum RMS amplitude on the transverse extension of the probed space time volume is shown in Fig. 4. The normalized increase of total noise, measured with respect to bare shot noise (right vertical axis), is plotted against the probe spot radius  $w_0$  (blue squares). Conversion to the vacuum electric amplitude  $\Delta E_{\text{vac}}$  (left vertical axis) has been carried out analogously to  $|\Psi_0(E)\rangle^2$  in Fig. 2B. The functional dependence expected from Eq. 5 is shown as a red line. The inset in Fig. 4 illustrates the data recorded at low beam cross sections a

linear scale to highlight the hyperbolic increase of vacuum fluctuations for the smaller space time volumes that we probed.

In our study, we directly monitored vacuum fluctuations without amplifying them. The only effective part  $\sum_{\Omega>0} \hat{a}_\Omega \hat{a}_\Omega^\dagger$  of the operator that extracts the variance of the field in Eq. 4 indicates that vacuum fluctuations correspond to photons, which spontaneously arise and vanish in the ground state  $\Phi_0$ . Time energy uncertainty demands that virtual excitations have a limited life time on the order of their oscillation cycle (32). The subcycle temporal resolution provided by the ultrashort probe ensures that we can directly detect effects originating from purely virtual photons. Phase matched copropagation of the vacuum field and probe inside the EOX maximizes those signals. But does this measurement influence the quantum vacuum at all? Based on the electro optic change of the refractive index  $\Delta n_p \sim r_{43} E_{\text{THz}}$ , the local multiterahertz field imprints a phase shift onto the ultrashort probe, which we detected. Because sum and difference frequency mixing occur simultaneously in this process (29), it requires no net transfer of energy, momentum, or angular momentum, and it even avoids modulation of the refractive index at frequencies  $\Omega/2\pi \ll \nu_p$ . Our second order nonlinear element operates far from resonance. Virtual driving of the transitions avoids problems with decoherence, distinguishing our experiment from detection approaches in quantum optics or circuit quantum electrodynamics in which resonant two level systems are involved (33). In consequence, our approach may be used to study the multi terahertz ground state while imposing negligible influence on it. Back action might arise only in third order: The nonlinear refractive index  $n_2$  generates a local anomaly of phase velocity copropagating with the intensity envelope of the probe, because  $\Delta n_2 \sim n_2 |E_p|^2$ . When  $N_p/w_0^2 t_p$  suffices to induce phase shifts of the multiterahertz field during passage through the EOX, depletion of the vacuum amplitude in the sampled space time volume and enhanced fluctuations in an adjacent interval are expected.

#### REFERENCES AND NOTES

- W. Vogel, D. G. Welsch, *Quantum Optics* (Wiley VCH, Weinheim, Germany, ed. 3, 2006).
- D. F. Walls, G. J. Milburn, *Quantum Optics* (Springer Verlag, Berlin, ed. 2, 2008).
- W. E. Lamb Jr., R. C. Retherford, *Phys. Rev.* **72**, 241–243 (1947).
- H. Casimir, *Proc. Kon. Ned. Akad. Wetensch. B* **51**, 793–795 (1948).
- E. P. Tryon, *Nature* **246**, 396–397 (1973).
- V. F. Mukhanov, H. A. Feldman, R. H. Brandenberger, *Phys. Rep.* **215**, 203–333 (1992).
- F. Schwabl, *Quantum Mechanics* (Springer Verlag, Berlin, ed. 4, 2007).
- Materials and methods are available as supplementary materials on Science Online.
- J. D. Jackson, *Classical Electrodynamics* (Wiley, New York, ed. 3, 1999).
- I. A. Walmsley, *Science* **348**, 525–530 (2015).
- R. Hanbury Brown, R. Q. Twiss, *Nature* **177**, 27–29 (1956).
- H. J. Kimble, M. Dagenais, L. Mandel, *Phys. Rev. Lett.* **39**, 691–695 (1977).
- P. Michler et al., *Nature* **406**, 968–970 (2000).
- B. Lounis, W. E. Moerner, *Nature* **407**, 491–493 (2000).

15. R. E. Slusher, L. W. Hollberg, B. Yurke, J. C. Mertz, J. F. Valley, *Phys. Rev. Lett.* **55**, 2409–2412 (1985).
16. L. A. Wu, H. J. Kimble, J. L. Hall, H. Wu, *Phys. Rev. Lett.* **57**, 2520–2523 (1986).
17. D. T. Smithey, M. Beck, M. G. Raymer, A. Faridani, *Phys. Rev. Lett.* **70**, 1244–1247 (1993).
18. A. I. Lvovsky *et al.*, *Phys. Rev. Lett.* **87**, 050402 (2001).
19. N. B. Grosse, T. Symul, M. Stobińska, T. C. Ralph, P. K. Lam, *Phys. Rev. Lett.* **98**, 153603 (2007).
20. A. M. Fox, J. J. Baumberg, M. Dabbicco, B. Huttner, J. F. Ryan, *Phys. Rev. Lett.* **74**, 1728–1731 (1995).
21. M. E. Anderson, M. Beck, M. G. Raymer, J. D. Bierlein, *Opt. Lett.* **20**, 620–622 (1995).
22. C. Silberhorn *et al.*, *Phys. Rev. Lett.* **86**, 4267–4270 (2001).
23. P. J. Mosley *et al.*, *Phys. Rev. Lett.* **100**, 133601 (2008).
24. Q. Wu, X. C. Zhang, *Appl. Phys. Lett.* **71**, 1285–1286 (1997).
25. A. Leitenstorfer, S. Hunsche, J. Shah, M. C. Nuss, W. H. Knox, *Appl. Phys. Lett.* **74**, 1516–1518 (1999).
26. K. Liu, J. Z. Xu, X. C. Zhang, *Appl. Phys. Lett.* **85**, 863–865 (2004).
27. C. Kübler, R. Huber, S. Tübel, A. Leitenstorfer, *Appl. Phys. Lett.* **85**, 3360–3362 (2004).
28. S. Namba, *J. Opt. Soc. Am.* **51**, 76–79 (1961).
29. G. Gallot, D. Grischkowsky, *J. Opt. Soc. Am. B* **16**, 1204–1212 (1999).
30. A. S. Moskalenko, C. Riek, D. V. Seletskiy, G. Burkard, A. Leitenstorfer, <http://arxiv.org/abs/1508.06953> (2015).
31. R. Loudon, P. L. Knight, *J. Mod. Opt.* **34**, 709–759 (1987).
32. C. Fürst, A. Leitenstorfer, A. Laubereau, R. Zimmermann, *Phys. Rev. Lett.* **78**, 3733–3736 (1997).
33. A. A. Clerk, M. H. Devoret, S. M. Girvin, F. Marquardt, R. J. Schoelkopf, *Rev. Mod. Phys.* **82**, 1155–1208 (2010).

#### ACKNOWLEDGMENTS

Support by the European Research Council (Advanced Grant 290876 “UltraPhase”), by Deutsche Forschungsgemeinschaft (SFB767), and by NSF via a postdoctoral fellowship for D.V.S. (award no. 1160764) is gratefully acknowledged.